Ferlins show tissue-specific expression and segregate as plasma membrane/late endosomal or trans-Golgi/recycling ferlins.

Gregory Michael Ian Redpath; Reece Andrew Sophocleous; Lynne Turnbull; Cynthia B Whitchurch; Sandra T Cooper

[1]Institute for Neuroscience and Muscle Research, Kid's Research Institute, Children's Hospital at Westmead, Sydney, NSW 2145, Australia,

[2]Discipline of Paediatrics and Child Health, Faculty of Medicine, University of Sydney, Sydney, NSW 2006, Australia, and

[3]Microbial Imaging Facility, the ithree institute, University of Technology Sydney, Ultimo, NSW 2007, Australia

*Address correspondence to: Sandra Cooper (sandra.cooper@sydney.edu.au).

Synopsis

Ferlins are an ancient family of Ca^{2+}-binding, multi-C2 domain vesicle fusion proteins. Of the six human ferlins, mutations in dysferlin cause muscular dystrophy and otoferlin cause deafness. We detail the tissue-distribution, subcellular localization and endocytic trafficking of the human ferlins. Dysferlin and myoferlin, type-I ferlins, localise to the plasma membrane and late endosomes, which display potential for occasional recycling. Otoferlin and Fer1L6, type-II ferlins, localise to dedicated recycling sub-compartments of the trans-Golgi network. We establish that type-I and type-II ferlins segregate into late-endosomal and recycling trans-Golgi compartments.

Abstract

Ferlins are a family of transmembrane-anchored vesicle fusion proteins uniquely characterized by 5-7 tandem cytoplasmic C2 domains, Ca^{2+}-regulated phospholipid-binding domains that regulate vesicle fusion in the synaptotagmin family. In humans, dysferlin mutations cause limb-girdle muscular dystrophy (LGMD2B) due to defective Ca^{2+}-dependent, vesicle-mediated membrane repair and otoferlin mutations cause non-syndromic deafness due to defective Ca^{2+}-triggered auditory neurotransmission. In this study, we describe the tissue-specific expression, subcellular localization and endocytic trafficking of the ferlin family. Dysferlin, myoferlin, and Fer1L6 are plasma membrane (PM) ferlins, whereas otoferlin and Fer1L5 localize predominantly to intracellular compartments. Studies of endosomal transit together with 3D-structured illumination microscopy reveals dysferlin and myoferlin are abundantly expressed at the PM and cycle to Rab7-positive late endosomes, supporting potential roles in the late-endosomal pathway. In contrast, Fer1L6 shows concentrated localization to a specific compartment of the trans-Golgi/recycling endosome, cycling rapidly between this compartment and the PM via Rab11 recycling endosomes. Otoferlin also shows trans-Golgi to PM cycling, with very low levels of PM otoferlin suggesting either brief plasma membrane residence, or rare incorporation of otoferlin molecules into the PM. Thus, type-I and type-II ferlins segregate as PM/late-endosomal or trans-Golgi/recycling ferlins, consistent with different ferlins mediating vesicle fusion events in specific subcellular locations.

This article has been accepted for publication and undergone full peer review but has not been through the copyediting, typesetting, pagination and proofreading process, which may lead to differences between this version and the Version of Record. Please cite this article as doi: 10.1111/tra.12370

Abbreviations: DYSF: dysferlin; **MYOF**: myoferlin; **$OTOF_N$**: neuronal otoferlin; **$OTOF_{Ub}$**: ubiquitous otoferlin; **DDK**: Flag epitope tag; **HEK293**: human embryonic kidney 293 cells; **IRES**: internal ribosome entry site; **WGA**: wheat germ agglutinin; **3D-SIM**: three-dimensional structured illumination microscopy; **ER**: endoplasmic reticulum; **GM130**: Golgi matrix protein of 130 kDa; **TGOLN2**: trans-Golgi network integral membrane protein 2; **LAMP1**: lysosomal associated membrane protein 1. **PM:** Plasma membrane.

Introduction

Ferlins are an ancient family of vesicle fusion proteins characterized by the unique structure of 5-7 cytoplasmic C2 domains (Ca^{2+}-regulated, phospholipid-binding domains), anchored by a C-terminal transmembrane domain (1). There are six mammalian ferlins - Fer1L1 (dysferlin), Fer1L2 (otoferlin), Fer1L3 (myoferlin) and Fer1L4-6. Type-I ferlins (dysferlin, myoferlin and Fer1L5) are defined by the presence of the DysF domain in the centre of the molecule (three C2 domains either side), an independently folding domain of unknown function (2, 3). In yeast, DysF domain containing proteins regulate peroxisome size and number (4). Type-II ferlins (otoferlin, Fer1L4 and Fer1L6) are defined by the absence of the DysF domain. All ferlins also contain Fer domains, conserved domains unique to the ferlin family that are yet to be structurally or functionally defined (5).

The unifying feature of ferlin animal models from invertebrates to humans, are pathologies linked specifically to defects in Ca^{2+}-dependent vesicle fusion (reviewed (1)). Ferlins are hypothesised to mediate vesicle fusion via their multiple C2 domains (1). C2 domains consist of around 100 amino acids and fold into a conserved, characteristic 8-stranded beta sheet structure (6). The synaptotagmin family of vesicle fusion proteins bear two C2 domains. Synaptotagmin-1 triggers synaptic vesicle fusion, and the crystal structures and Ca^{2+}- and phospholipid-binding properties of the two C2 domains have been well characterized (6, 7). In synaptotagmin-1, C2B binds Ca^{2+} in the top loop regions via a binding pocket of conserved aspartic acid residues, acquiring a positive charge that enables loop insertion into negatively-charged phospholipid membranes (8). Insertion of Ca^{2+}-bound C2 domain loops into phospholipid membranes is proposed to induce membrane curvature and help overcome the energetic barrier for vesicle fusion with the target membrane (9).

The structures of dysferlin C2A (10) and otoferlin C2A (11) have been solved. Interestingly, alternate splicing of dysferlin exon 1 leads to two variant $C2_A$ domains. Structural and thermodynamic analyses indicate the canonical C2A domain functions as a Ca^{2+}-dependent, phospholipid-binding domain. In contrast, due to intrinsic positive electrostatic charges on the outer surface of $C2A_{v1}$, this domain appears as a structural mimic of Ca^{2+}-bound C2A, and is likely to be Ca^{2+} -independent under physiological conditions (10). In contrast, otoferlin C2A was not shown to bind Ca^{2+} or phospholipid membranes, consistent with a structural difference observed in one of the top loops that typically contribute to Ca^{2+} coordination in other C2 domains (11). Therefore, otoferlin C2A does not possess a positively charged groove thought to mediate interaction with negatively charged lipids (11). Studies of isolated C2 domains from dysferlin (10, 12, 13) and otoferlin (14) show properties of Ca^{2+}- and phospholipid binding, though structural data was not available to demonstrate whether purified domains have assumed a classical C2 β-sheet fold.

Mutations in dysferlin cause limb-girdle muscular dystrophy type 2B (15, 16). Dysferlin knockout mouse muscle fibres display a primary defect in Ca^{2+}-dependent membrane repair (17), a process involving Ca^{2+}-triggered exocytosis to 'patch' membrane wounds (18). Dysferlin-laden vesicles show Ca^{2+}-regulated accumulation at injury sites and appears to fill membrane lesions in human myotubes (19) and zebrafish skeletal muscle (20), consistent with dysferlin mediating vesicle fusion at sites of membrane injury. In humans, otoferlin mutations cause an inherited form of profound, non-syndromic deafness (21, 22). Otoferlin-knockout mice are also profoundly deaf, and show a primary defect in Ca^{2+}-dependent synaptic exocytosis from the basolateral membrane of inner hair cells, abolishing neurotransmitter release to the auditory nerve (23).

No disease-causing mutations have yet been identified in myoferlin, Fer1L4, Fer1L5 or Fer1L6. Myoferlin knockdown reduces endocytosis and subsequent degradation of growth-factor receptors (24), and reduces breast cancer cell line migration velocity (25). Myoferlin expression is upregulated in breast cancer biopsies (26), lung carcinoma (27), pancreatic adenocarcinoma (28), breast ductal adenocarcinoma (24) and chronic muscle disease in mice (29, 30). Fer1L4 mRNA is expressed in healthy stomach tissue and downregulated in gastric cancer samples, where it is proposed to be a pseudogene (31, 32).

In the synaptotagmin family there are thirteen members, with different synaptotagmins mediating vesicle fusion in specific tissues (33, 34) or subcellular compartments (35). Synaptotagmin-1 mediates fusion of neurotransmitter containing vesicles to synapses in nerves (10, 36, 37), while synaptotagmin-VII mediates insulin-containing and glucagon-containing vesicle fusion in pancreatic islet cells (38, 39). We hypothesise that analogous to the synaptotagmins each ferlin will mediate vesicle fusion events involving discrete cargo in specific tissues and at specific subcellular locations.

In this study, we describe the tissue-specific expression, sub-cellular localization and endocytic trafficking of the human ferlin family. We show that dysferlin, myoferlin, and Fer1L6 are plasma membrane ferlins, whereas otoferlin and Fer1L5 predominantly localize to intracellular compartments. Studies of endosomal transit together with 3D-structured illumination microscopy (3D-SIM (40)) reveal that dysferlin and myoferlin transit to late endosomes, whereas otoferlin and Fer1L6 are trans-Golgi/recycling ferlins. Our data is consistent with different ferlins mediating vesicle fusion events in specific subcellular locations.

Results

Tissue-specific expression of each ferlin in human tissues.

We investigated the expression of each of the six mammalian ferlins across 12 human tissues, using a semi-quantitative PCR approach. We utilized two sets of primers specific for each ferlin, a pair amplifying the 5' region of the gene (with one primer within the 5' untranslated region, UTR, not shown) and a second pair amplifying the 3' region of the gene (with one primer within the 3' UTR). Results from the 3' primer pair are shown in Figure 1, employing 30, 35 and 40 cycles of amplification to provide a rudimentary standard curve and to control for saturation.

Dysferlin and myoferlin mRNAs are expressed ubiquitously, detected in all tissues analyzed (Figure 1A, DYSF, MYOF). Alternate splicing confers neuronal-specific and ubiquitous transmembrane domains for otoferlin (Choi et al., 2009), regulated by the inclusion or exclusion of exon 47 (Figure 1B). Exon 47 is expressed only in brain (Figure 1A, OTOF, higher band asterisked), conferring a neuronal specific transmembrane domain ($Otof_N$). Interestingly, otoferlin mRNA bearing the alternate transmembrane domain encoded by exon 48 (where exon 47 is absent) is detectable in all tissues apart from skeletal muscle and kidney (Figure 1A, OTOF, lower band). We refer to this otoferlin transcript as ubiquitous otoferlin ($Otof_{Ub}$).

Fer1L4, L5 and L6 show more restricted patterns of expression. Fer1L4 is annotated as a non-protein coding RNA (NCBI Gene: 80307; ENSEMBL ENSG00000088340). Fer1L4 mRNA expression was observed primarily in the stomach (Figure 1A, L4). Fer1L5 expression was largely restricted to the pancreas (Figure 1A, L5), with other tissues analyzed generally showing low or absent expression of Fer1L4 or L5. Interestingly, Fer1L5 expressed in the pancreas is alternately spliced, removing exon 51 (Figure 1A, B). In Fer1L5 isoform 1, exon 51 encodes for the transmembrane domain. Splicing directly from exon 50 to 52 results in a +1 frame-shift, introducing an alternate stop codon early in exon 52 and removing the predicted luminal domain of Fer1L5 (Figure 1B, C). In stomach and esophagus, where low levels of Fer1L5 are expressed, doublet bands are observed with the 3' primer pair; the upper band includes exon 51, whereas the lower band excludes exon 51 (Figure 1A, L5: stomach, esophagus). Fer1L6 expression is highest in heart, kidney and stomach, with lower levels observed in lung, liver, pancreas, thymus and colon (Figure 1A, L6). These expression data are consistent with RNA sequencing data recently available with open access;
http://www.gtexportal.org; http://www.proteinatlas.org;
http://www.ncbi.nlm.nih.gov/IEB/Research/Acembly.

Dysferlin, myoferlin and Fer1L6 are plasma membrane ferlins, whereas otoferlin and Fer1L5 are predominantly intracellular

We have shown previously that dysferlin localizes to the plasma membrane and to endosomal vesicles, using luminal and cytoplasmic epitopes to verify membrane topology (41). Plasma membrane localization has been previously confirmed for myoferlin (42), and there are no studies confirming the precise subcellular localization of other ferlins. We derived ferlin expression constructs with C-terminal epitope tags (MycHis for dysferlin or MycDDK for myoferlin, otoferlin, Fer1L5 and Fer1L6), which are luminal for intracellular ferlins or extracellular for plasma membrane ferlins. These epitope tags allow us to determine whether a ferlin is expressed at the plasma membrane, and to track endosomal retrograde trafficking. No commercial antibodies are available to the short

luminal domain (10-20 amino acids) of any ferlin. Based on the limited expression profile of Fer1L4 and difficulty deriving such large expression constructs, we did not generate a Fer1L4 construct for localization studies.

To determine which mammalian ferlins target the plasma membrane, we performed surface labelling of live cells with anti-Myc^{647} (for flow cytometry) or anti-Myc^{555} (for confocal microscopy) at 8^{o}C for 90 mins. We studied transfected HEK293 epithelia and C2C12 myoblasts, with consistency of observations between these disparate cell types. For simplicity, only results from HEK293 cells are presented in Figure 2.

Dysferlin, myoferlin and Fer1L6 are readily detected at the plasma membrane, whereas otoferlin and Fer1L5 are predominantly intracellular (Figure 2). For flow cytometry, live cells were gated based on exclusion of propidium iodide, and transfected cells were gated by expression of EGFP via the internal ribosome entry site (IRES) within the expression vector. Figure 2A*i* shows flow cytometry quantification of levels of surface-bound anti-Myc^{647}, relative to the EGFP expressed from the same mRNA, over three experiments. Dysferlin has a MycHis tag, compared to a MycDDK tag for myoferlin and Fer1L6. Anti-Myc may exhibit different affinities for the different epitope tags, therefore relative plasma membrane levels of dysferlin cannot be directly compared to myoferlin and Fer1L6. Figure 2A*ii* shows the normal distribution of surface-bound anti-Myc^{647} among the pool of transfected cells from duplicate samples in a single experiment. Western blotting from replicate samples performed on the same day confirms ferlin expression in cell pellets (Figure 2A*iii*). We obtained no evidence for cell surface expression of Fer1L5, whereas low levels of the ubiquitous isoform of otoferlin (OTOF$_{Ub}$) can be detected at the plasma membrane by flow cytometry (confirmed using an anti-Flag binding curve shown in Supplementary Figure 1A). Representative dot-plots of the flow cytometry data are displayed in Supplementary Figure 1A.

To confirm plasma membrane localization, transfected HEK293s used for flow cytometry were also plated onto coverslips. Confocal microscopy of live cells surface-labeled with anti-Myc^{555} confirmed robust plasma membrane expression of dysferlin, myoferlin and Fer1L6 in transfected cells expressing EGFP (Figure 2B DYSF, MYOF, L6). We observed weakly positive cell surface labeling for anti-Myc^{555} in cells transfected with ubiquitous otoferlin (Figure 2B, OTOF$_{Ub}$). We could not detect plasma membrane labeling for Fer1L5 or neuronal otoferlin (Figure 2B OTOF$_{N}$, L5), consistent with flow cytometry results.

We next used 3D-structured illumination microscopy (3D-SIM) to compare the surface localization of each ferlin to the plasma membrane marker wheat germ agglutinin (WGA). In live cells, dysferlin, myoferlin and Fer1L6 intercalate with WGA, indicating that the ferlin C-terminus is in the same plane of the plasma membrane as the WGA-labeled glycosylated proteins (Figure 2C). In permeabilised cells, ubiquitous and neuronal otoferlin and Fer1L5 are below the plane of the plasma membrane, consistent with intracellular localization and concordant with our flow cytometry and confocal microscopy results (Figure 2C).

In summary, dysferlin, myoferlin and Fer1L6 are plasma membrane ferlins, Fer1L5 is an intracellular ferlin, and only low levels of otoferlin are present at the plasma membrane.

Different ferlins localize to different compartments of the secretory pathway.

Confocal microscopy of fixed and permeabilised HEK293 epithelia, C2C12 myoblasts and Cos-7 fibroblasts transfected with our ferlin expression constructs shows that each ferlin has a distinct subcellular localization (Figure 2D). Detailed co-localization studies with subcellular markers for calreticulin (endoplasmic reticulum), GM130 (cis-Golgi apparatus), TGOLN2 (also known as TGN38/46, trans-Golgi network), Rab5 (early endosomes), Rab7 (late endosomes) or LAMP1 (lysosomes) are presented in Figures 4, 5, 6 and 7. As the yeast DysF domain-containing proteins Pex30p and Pex31p localize to peroxisomes in yeast (4) we examined ferlin localization to peroxisomes using the peroxisome marker Pex-14. No human ferlin co-localized with Pex14 labeled compartments, and therefore this data is not presented.

Dysferlin and myoferlin show widespread labeling of the plasma membrane and bright labeling of vesicular puncta within the perinuclear region and cytoplasm (Figure 2D). Consistent with export to the plasma membrane, we observed some co-localization of dysferlin and myoferlin with secretory pathway markers (calreticulin-ER, GM130-Golgi, TGOLN2-trans-Golgi; Figure 3). However, more prominent co-localization was consistently observed with endosomal markers Rab5 and Rab7 (Figure 4, Supplementary Figure 2). Myoferlin showed strong co-localization with large Rab7-positive endosomes within in the perinuclear region and also in the cell periphery (Figure 4B, Supplementary Figure 2B). Dysferlin and myoferlin endosomes have a clearly observable lumen and range in size from several hundred nanometers to >1 micron - comparable in size to LAMP-1 positive organelles (Figure 4A, B, 3D-SIM; resolution of single z-plane ~300 nm). Despite abundant co-labeling of dysferlin and myoferlin vesicles for late endosomal marker Rab7, we observed only occasional co-

labeling with the lysosomal marker LAMP-1 in HEK293, C2C12 and Cos-7 cells (Figure 4A, B, LAMP1; Supplementary Animation 1A and B, Supplementary Figure 2). Thus dysferlin and myoferlin label a pool of large Rab7-positive late endosomes discrete from LAMP1-positive lysosomes.

Otoferlin shows limited co-labeling with ER markers, some co-labeling with GM130 and more comprehensive overlap with the trans-Golgi marker TGOLN2 (Figure 5). We observed a very similar sub-cellular localization between the ubiquitous ($OTOF_{Ub}$) and neuronal isoforms of otoferlin ($OTOF_N$ - shown in Supplementary Animation 1B). 3D-SIM resolves that $otoferlin_{Ub}$ and TGOLN2 co-label a web of interconnected tubules (Figure 5, 3D-SIM). These intersecting tubules are within the same z-plane and clearly apparent within the reconstructed 3D-SIM image of the trans-Golgi network (Supplementary Animation 1C). Generally otoferlin and TGOLN2 each labels discrete segments of this tubular network, with direct overlay of each fluorescent signal observed at junctions of intersecting tubules (Figure 5, 3D-SIM, Supplementary Animation 1C). Otoferlin resides on the cytoplasmic face of the trans-Golgi stacks, while TGOLN2 resides on the nuclear side (Figure 5, 3D-SIM). These data suggest otoferlin and TGOLN2 both localize to the trans-Golgi network, but separately label closely associated yet discrete sub-compartments.

Fer1L6 shows highly concentrated localization to a distinct perinuclear structure that is partially co-labeled by TGOLN2 (Figure 6A, TGOLN2, 3D SIM, Supplementary Figure 3). Concentrated localization of Fer1L6 to this specific compartment was striking in lesser-transfected cells which show a distinct, piercing spot adjacent to the nucleus, through to highly over-expressing cells where this compartment expands and appears to induce a furrow in a nucleus (Figure 6B). Studies using the nuclear envelope marker Lamin A/C indicate the Fer1L6 compartment is discrete from, but adjacent to the nuclear envelope (Figure 6C, left panel).

In a single z-plane, the Fer1L6 compartment contains TGOLN2 positive regions, but is not entirely TGOLN2 positive. Conversely some, but not all, TGOLN2 staining is present in the Fer1L6 compartment (Figure 6A, TGOLN2 confocal inset). 3D-SIM reveals the Fer1L6 compartment consists of two connected stacks (Supplementary Animation 1D). TGOLN2-positive vesicles are present within and in-between the stacks of Fer1L6 (Supplementary Animation 1D), highlighting the interplay between the Fer1L6 compartment and trans-Golgi network. It is important to note that although Fer1L6 labels the plasma membrane (Figure 2B), when imaging permeabilized cells, the intensity of labeling of the perinuclear compartment is so great that imaging must be performed with low laser power, whereby the plasma membrane labeling appears faint.

Fer1L6 shows a high degree of co-localisation with endocytosed transferrin, which labels the recycling endosome. To confirm that Fer1L6 localizes to a trans-Golgi/recycling compartment, we disrupted the Golgi apparatus with brefeldin-A. Brefeldin-A treatment of Golgi apparatus disperses cis-Golgi markers throughout the ER and cytoplasm, while TGOLN2 collapses to the perinuclear microtubule organization complex (43). Brefeldin-A treatment for 2 hours disrupts the Golgi apparatus, dispersing GM130 staining throughout the cell (Figure 6D, left two panels). FerL6 localization is relatively unperturbed by brefeldin-A, consistent with FerL6 localization to specific sub-compartments of the trans-Golgi apparatus and recycling endosome (Figure 6D, right panel).

The localization of Fer1L5 appears reticular by confocal microscopy and we initially surmised this likely represented the endoplasmic reticulum (ER). However, evidence for fluorescent overlay with calreticulin (Figure 7, calreticulin) or calnexin (data not shown) was weak, by confocal microscopy and 3D-SIM. Labeling for ER markers and Fer1L5 were closely associated, but did not completely overlay. Fer1L5 also did not co-label with GM130 (Figure 7), TGOLN2 or LAMP1 (data not shown), and its localization remains uncertain.

Endocytic trafficking of the ferlins.

The C-terminal epitope tag on the luminal domain of our ferlin expression constructs allows us to specifically examine retrograde trafficking for plasma membrane ferlins. Live cells were incubated with anti-Myc at 37°C, which binds to the cell surface epitope tag and is co-endocytosed with the ferlin. Figure 8A image depicts the endocytic trafficking representative of each ferlin. As Fer1L5 is not at the plasma membrane, it was used to control for specificity of the retrograde tracing approach, confirming anti-Myc antibodies are not taken up by non-specific means (Figure 8A, Fer1L5). Retrograde tracing experiments recapitulate features of total intracellular staining for each ferlin (compare with Figure 2D). Specifically dysferlin and myoferlin label cytoplasmic endosomes, Fer1L6 shows concentrated return to a distinct perinuclear compartment and otoferlin undergoes retrograde traffic to a broader perinuclear compartment.

Retrograde tracing of dysferlin and myoferlin (using antibody uptake experiments ranging from 15 – 90 minutes) shows transit in Rab7 late endosomes and eventual labeling of a small population of LAMP-1 positive lysosomes (Figure 8B, dysferlin and myoferlin). 3D-SIM clarified that dysferlin and myoferlin were within the lysosomal

membrane of some LAMP-1 positive organelles and intraluminal within others (Figure 8B, dysferlin and myoferlin and Supplemental Animation 2A and B). Data from retrograde tracing was consistent with total intracellular staining, with co-localization of dysferlin and myoferlin to Rab7 positive organelles a predominant feature of both intracellular staining and endocytic labeling (Figure 9A, Figure 4 Rab7). Collectively, our results suggest dysferlin and myoferlin may play dedicated roles within the late endosomal pathway, rather than merely transiting this route on their way to degradation.

In contrast to dysferlin and myoferlin, antibody uptake experiments with Fer1L6 and otoferlin results in endocytic transit to the trans-Golgi apparatus (Figure 8B). As observed with total intracellular staining (Figure 5), retrograde labeling of otoferlin highlights a trans-Golgi compartment closely adjacent to, yet separate from, TGOLN2 (Figure 8B, otoferlin; Supplementary Animation 2C). Retrograde labeling of Fer1L6 intensely highlights a specific sub-compartment of the trans-Golgi network (Figure 8B, Fer1L6, Supplementary Animation 2D). TGOLN2 labels vesicles in and *between* Fer1L6 stacks, consistent with intracellular staining. 3D-SIM analyses confirm the Fer1L6 stacks are intimately associated with the trans-Golgi network, but separate from the trans-Golgi structure/stack labeled by TGOLN2.

As our evidence suggests Fer1L6 shuttles to and from a recycling sub-compartment of the trans-Golgi stack, we explored whether Fer1L6 showed association with Rab11a-positive recycling endosomes. Endocytic tracing experiments reveal that Fer1L6 shows abundant co-localization with Rab11a-endosomal vesicles in the cell periphery (Figure 9B, Fer1L6 inset). Thus, Fer1L6 transits to a larger perinuclear organelle co-labeled by Rab11a (Figure 9B, white arrows), transferrin uptake (Figure 9C) and TGOLN2. Therefore, we believe the Fer1L6 compartment that we observe in both intracellular staining and endosomal uptake represents the recycling endosomal compartment. Fer1L6 transit to the recycling endosomal compartment is very rapid, occurring following addition of anti-Myc to the media for as little as 10 minutes (Figure 9B, Fer1L6).

Retrograde tracing of otoferlin, myoferlin and dysferlin (with anti-Myc) together with endocytosed transferrin[594] also showed some overlay of a perinuclear compartment, suggesting these ferlins may also transit the recycling endosome (Figure 9). Similarly, in contrast to Fer1L6, retrograde tracing of otoferlin did not show strong co-labeling of peripheral vesicles positive for Rab11a-GFP (data not shown). Furthermore, co-uptake experiments with otoferlin (anti-Myc) and anti-TGOLN2 showed that although both proteins undergo retrograde transit back to the trans-Golgi network, we could not detect evidence for co-transit within the same endosomal vesicle population en route to the trans-Golgi. The precise endocytic pathway of otoferlin remains to be elucidated.

Discussion

In this study, we have characterized the mRNA expression, subcellular localization and endocytic trafficking of the human ferlin family in three cell lines of different lineages (HEK epithelia, C2C12 myoblasts and Cos-7 fibroblasts. Though we acknowledge the caveat of overexpression systems, in this case, antibodies to the luminal domain of ferlins required to trace endosomal passage are not available. Comparing each of the ferlins to one another in different cell types, our results strongly suggest that different ferlins target different compartments of the secretory pathway. We establish the ferlins fall into two distinct categories: dysferlin and myoferlin are plasma membrane/endosomal ferlins, while otoferlin and Fer1L6 are trans-Golgi/recycling ferlins (Figure 10).

Dysferlin and myoferlin are expressed at the plasma membrane and transit to the late-endosomal pathway. Although both dysferlin and myoferlin abundantly co-label Rab7 positive late endosomes, this is a particularly dominant feature for myoferlin. The high level of co-localization with late endosomal compartments lead us to expect a greater proportion of myoferlin and dysferlin to be present within lysosomes, but this was not the case. At the lysosome, dysferlin and myoferlin are present both within the lysosomal membrane and lumen. We were specifically interested in this localization as it illuminates whether these two ferlins have eventuated at the lysosome via multivesicular bodies (where they would be intraluminal) or have been present within the membrane of the endosomal vesicle as it matures.

There is mounting evidence supporting functional roles for dysferlin and myoferlin in the endo-lysosomal pathway. Dysferlin null-myoblasts have double the number of lysosomes in comparison to wild-type myoblasts (44), suggesting dysferlin may play a regulatory role in lysosomal biogenesis or maturation. In dysferlin-null myoblasts, insulin growth-factor receptor (IGFR) shows greater accumulation within lysosomes compared to wild-type myoblasts (44), implicating a role for dysferlin in receptor trafficking through the endo-lysosomal pathway. Myoferlin knockdown in MDA-231 epithelial breast cancer cells decreases epidermal growth-factor receptor (EGFR) degradation, diminishing the cell proliferation response of epidermal growth factor (24). Myoferlin

knockdown does not reduce EGFR endocytosis but prevents EGFR degradation (24), indicating that myoferlin regulates transit of endosomal cargo to the lysosome. We propose that dysferlin and myoferlin are localised primarily within Rab7 late endosomes to exert functional roles in late-endosomal to lysosomal trafficking, as opposed to being trafficked to the lysosome exclusively for degradation.

In contrast to dysferlin and myoferlin, otoferlin and Fer1L6 show little labeling of endo-lysosomal organelles, and instead localise to trans-Golgi and recycling networks. However, while Fer1L6 is abundantly expressed at the plasma membrane, only very low levels of otoferlin$_{Ub}$ are detectable at the plasma membrane. Fer1L6 shows profound and restricted localization to a brefeldin-A resistant region of the trans-Golgi/recycling endosomal compartment that is partially co-labeled by TGOLN2 and Rab 11a and abundantly labeled by endocytosed transferrin. Overexpression of Fer1L6 appears to induce expansion of this recycling compartment to such a degree that it deforms the nucleus, suggesting Fer1L6 may regulate its biogenesis. Otoferlin also localizes to a compartment of the trans-Golgi network that is immediately adjacent to, yet also distinct from TGOLN2-labeled membranes. While Fer1L6 endocytoses via Rab11a-positive endosomes to what we believe to be the Rab11a/TGOLN2 recycling endosomal compartment, otoferlin endocytoses to the trans-Golgi network via a different endocytic pathway. Thus, our data suggests otoferlin and Fer1L6 each recycle independently between different sub-compartments of the trans-Golgi network and the plasma membrane (Figure 10).

The trans-Golgi recycling features we identify for ubiquitous otoferlin are consistent with roles defined for otoferlin in synaptic exocytosis (23) and synaptic vesicle recycling (45) in cochlear inner hair cells. It is this ubiquitous otoferlin isoform bearing the transmembrane domain encoded by exon 48 that is expressed in the human cochlear (46). Otoferlin endogenously expressed within cochlear inner hair cells has previously been reported to localise to the Golgi apparatus (47), Rab8b-positive trans-Golgi compartments (48) and both apical and basolateral plasma membrane compartments (23, 49).

We were surprised to be able to effectively label the endosomal passage of otoferlin by antibody uptake experiments, given the very low levels of plasma membrane labeling. Perhaps rather than reflecting rare incorporation of otoferlin molecules into the plasma membrane, our data might suggest the exocytosis and endocytosis of otoferlin are closely coupled, resulting in only transient residence of otoferlin at the plasma membrane. Ours are only anecdotal observations, but perhaps relevant to expanding evidence implicating dual roles for otoferlin in the closely coupled exocytosis and recycling of synaptic vesicles in the cochlear.

Our data are broadly consistent with previously published reports of ferlin subcellular localisation. We have previously shown dysferlin co-labels syntaxin-4-positive and caveolin-3-positive endosomes in C2C12 and primary human myotubes (41). Dysferlin and myoferlin have also been identified in GM130-positive Golgi compartments in primary lung epithelia (50) and cancer cell lines (myoferlin) (27), and in cytoplasmic puncta in mouse myoblasts (51-53) and human breast cancer cell lines(24); consistent with the endosomal localization we observe, though endosomal markers were not specifically studied. Endogenous otoferlin co-localises with the trans-Golgi t-SNARE syntaxin-16 in inner hair cells (54). Otoferlin expressed in HEK293 cells co-localizes with the trans-Golgi Rab8b (48), consistent with our study.

Fer1L5 is similarly reported to show labeling of fine cytoplasmic tubules in mouse primary myoblasts (55, 56), and appears generally cytoplasmic in C2C12 (53). We did not observe the same intense patches of endogenous FerL5 labeling near or at the plasma membrane reported in C2C12 (53), though this labeling pattern was also not documented in primary myoblasts studied by the same authors (55, 56). Discrepancies between the precise intracellular localization of Fer1L5 in different models may relate to the antibody employed, the specific Fer1L5 isoform expressed (in our case human Fer1L5 NM_001293083.1) or intrinsic differences in the trafficking machinery in different cell types. Importantly, we could find no evidence for plasma membrane expression of Fer1L5 in HEK293, C2C12 or Cos7, and although Fer1L5 localization can be altered in absence of the endocytic recycling protein EHD1 (56), C2C12 express EHD1 and other members of the EHD family (53) and thus EHD proteins were not explored specifically as a basis for lack of export to the plasma membrane. In all three cell lines Fer1L5 staining appeared reticular but did not precisely co-label with ER markers calreticulin or calnexin by high resolution 3D-SIM, nor other markers of the secretory pathway, and thus we were unable to accurately refine its intracellular locale. No studies have investigated Fer1L6 sub-cellular co-localization to date, with our data presenting Fer1L6 as an interesting new marker of the TGN/recycling endosome.

In conclusion, our study has identified a discrete split in endocytic trafficking routes between type-I (dysferlin and myoferlin, endo-lysosomal) and type-II (otoferlin and Fer1L6, trans-Golgi to plasma membrane recycling) ferlins. Structurally, the major difference between type-I and type-II ferlins lies in type-I ferlins possessing a DysF domain. No function has yet been attributed to the DysF domain, and we will now explore whether the DysF domain plays a role in endo-lysosomal targeting. Our study represents the first in-depth characterization of the

sub-cellular localization and trafficking of the human ferlin family. We establish that dysferlin and myoferlin transit the plasma membrane to late endosomes, otoferlin recycles to and from the trans-Golgi network and Fer1L6 recycles to and from a trans-Golgi compartment via recycling endosomes. Defining specific tissue-specific expression and subcellular localization for each ferlin family member are important first steps to begin to address the different cellular cargo that may be regulated by the secretory and endocytic roles of this ancient family of vesicle fusion proteins.

Materials and Methods

Cell Culture

HEK293 and Cos-7 cells were cultured in DMEM (Life Technologies) with 10% FBS (Life Technologies) and 1:200 Gentamycin (Life Technologies). C2C12 myoblasts were cultured in 1:1 DMEM/F12 (Life Technologies) with 15% FBS and 1:200 Gentamycin.

Transfection

HEK293 cells were transfected with calcium phosphate or PEI (polyethylenimine Max, Polysciences) in 10 cm^2 dishes (BD Falcon). Cos-7 cells were transfected with Lipofectamine® 3000 (Life Technologies) in 3 cm^2 dishes. C2C12 myoblasts were transfected using GeneJuice® (Merck). For calcium phosphate, 100 µL of 0.25 M $CaCl_2$ (Sigma-Aldrich), 4 µg DNA and 100 µL of BES solution (50 mM BES, 280 mM NaCl, 1.5 mM $NaHPO_4{\cdot}7H_2O$ [Sigma-Aldrich]) was mixed and incubated at room temperature for 15 min prior to adding dropwise to cells. For PEI transfection, 8.3 µL 1 $mg.mL^{-1}$ PEI, 3 µg DNA and 200 µL of 0.9% NaCl (Baxter) was mixed and incubated at room temperature for 15 min prior to adding dropwise to cells. Dishes were transfected for 8 hours prior to transfer of cells to coverslips. For Lipofectamine® 3000, 7.5 µL of Lipofectamine® 3000 reagent was mixed with 125 µL of Opti-MEM® medium (Life Technologies) and was added to a master mix containing 125 µL of Opti-MEM®, 3.75 µg of DNA and 5 µL of P3000™ reagent and incubated at room temperature for 5 minutes prior to adding dropwise to cells. For GeneJuice® transfection, 1.5 µL GeneJuice® and 50 µL of Opti-mem® were mixed for 5 minutes at room temperature. 0.5 µg DNA was added and incubated for 10 minutes, followed by dropwise addition to coverslips. For co-transfection of Rab5/11a-EGFP, 2.75 µg of ferlin DNA and 250 ng of Rab5/11a-EGFP were used to minimize the effect of Rab over-expression on early and recycling endosomal pathways.

Immunocytochemistry

For all immunocytochemistry protocols, cells were plated on Number 1 thickness glass coverslips (TAAB Laboratory Equipment LTD) coated in poly-D-lysine (Sigma Aldrich) and mounted using ProLong Gold antifade reagent (Life Technologies).

Cell surface staining: Coverslips were incubated in rabbit anti-Myc (Abcam) diluted in 2% BSA in HBSS (blocking buffer) (Life Technologies) at 8°C for 1.5 hours. Following blocking, coverslips were incubated in anti-rabbit^{555} diluted in block at 8°C for 1 hour. Cells were then fixed in 3% PFA (Sigma Aldrich) and mounted as above.

Antibody Endocytosis: Rabbit or mouse anti-Myc was diluted in 37°C DMEM + 10% FBS and used to replace coverslip growth media. Following antibody incubation, coverslips were acid-washed in 0.5 M glycine (Sigma Aldrich) (pH 2.2) and fixed in 3% ice cold PFA. Cells were permeabilised with 0.1% saponin (Sigma Aldrich) and incubated in the indicated organelle marker antibody diluted in blocking buffer at room temperature for 1.5 hours. Coverslips were incubated with anti-mouse^{488} and anti-rabbit^{594} for 1 hour at room temperature, followed by DAPI for 10 minutes. Coverslips were then mounted as above.

Intracellular Staining: Coverslips were fixed in 3% PFA and permeabilised in 0.15% triton (Sigma Aldrich) (or 0.2% saponin for LAMP1 or 0.3% triton for Rab7). Coverslips were incubated in rabbit (Abcam) or mouse (Santa Cruz) anti-Myc and the indicated organelle marker antibody diluted in blocking buffer at room temperature for 1.5 hours. Coverslips were incubated with anti-mouse^{488} and anti-rabbit^{594} for 1 hour at room temperature, followed by DAPI for 10 minutes. Coverslips were then mounted as above.

Microscopy: All microscopy was undertaken using a Leica SP5 confocal microscope, or on a DeltaVision OMX V3 Blaze 3D structured illumination microscope (57) where indicated.

Flow Cytometry

Ferlin-pIRES2 EGFP transfected HEK293 cells were trypsinised and replated for 2 hours. Cells were then removed from plates with Versene^{TM} (Life Technologies) and pelleted. Cell pellets were resuspended in rabbit

anti-Myc in HBSS with 2% FBS for 1.5 hours at 10°C. Cells were then pelleted and washed, and resuspended in anti-rabbit^{647} (Life Technologies) in HBSS with 2% FBS for 1 hour at 10°C. Cells were again pelleted, washed and resuspended in HBSS with 1:200 propidium iodide (Life Technologies), following which cells were measured using a BD LSRII flow cytometer with FACS Diva software.

Western Blot

Cell pellets were lysed in RIPA buffer and separated on a 4-12% SDS-PAGE gel (Life Technologies). Protein was transferred onto PVDF membrane (Merck-Millipore). Membranes were blocked in 5% skim milk in PBS+ Tween-20 (block) and incubated in primary antibody at 4°C overnight, then HRP-conjugated secondary antibody (Thermo-Fischer Scientific) for 2 hours at room temperature. Blots were developed using ECL reagent (GE Healthcare).

Polymerase Chain Reaction

PCR was carried out for 30, 35 and 40 cycles with 58°C annealing and 40 second extension (70 second for GAPDH) using Taq DNA polymerase (Life Technologies). cDNA was sourced from Clontech (Human MTC Panel 1, Immune Panel and Gut Panel). Primers were designed to the 3` of each ferlin using Primer 3.0 and synthesized by Sigma-Aldrich.

Dysferlin Fwd: CAAGCTGGAAATGACCTTGG,
Dysferlin Rev: GCCTAGGAGGTCTGGAGGAG.
Otoferlin Fwd: AGGCAGAGAAGAACCCAGTG,
Otoferlin Rev: AAGCCACTGAAAGGAAATGC.
Myoferlin Fwd: CATGAACCCCAAGCTGGAC,
Myoferlin Rev: TGCAAACGTTGCTTGTTGG.
Fer1L4 Fwd: AAAGCAGAGGAGGAGGAAGG,
Fer1L4 Rev: GGGTGAGTGTCCAAGGTCAG.
Fer1L5 Fwd: CTGGAGATTCTGTCAGAGAAGG,
Fer1L5 Rev: GTTGGTAGCAGGAGGAAAGC.
Fer1L6 Fwd: CTGTTGGAAAAGCCCGAAAG,
Fer1L6 Rev: CCAAGAAGGGTTGATCTGTCC.

All PCR products were excised, purified (QiaexII Gel Purification Kit, Qiagen) and sequenced by the Australian Genome Research Foundation to confirm product specificity.

Antibodies and Fluorescent reagents

Rabbit anti-myc, 1:500 (surface and endosomal uptake), 1:4000 (intracellular) (Abcam); mouse anti-myc 9E10 1:100 (uptake), 1:500 (intracellular) (Santa Cruz); LAMP1 1D4B, 1:100 (Hybridoma Bank); LAMP1 4A3, 1:100 (Hybridoma Bank); TGOLN2/TGOLN2, 1:4500 (intracellular) or 1:250 (endosomal uptake) (Prestige Antibodies/Sigma Aldrich); Pex14, 1:1000 (Prestige Antibodies/Sigma Aldrich); GM130, 1:250 (BD Bioscience); Calreticulin 1:500 (Chemicon International); Calreticulin 1:200 (Novus Biological); Rab7 1:25 (Cell Signaling Technologies); EGFP (1:250); Transferrin from human serum^{594}, 100 µg.mL^{-1} (Life Technologies), Wheat germ agglutinin (WGA)^{488} 1:500 (Life Technologies); 4',6-diamidino-2-phenylindole (DAPI) 1:5000 (Life Technologies); anti-mouse^{488}, 1:200 (Life Technologies); anti-mouse^{594}, 1:200 (Life Technologies); anti-rabbit^{647}, 1:200 (Life Technologies).

Expression Constructs and Cloning

pcDNA4-EGFP-Dysferlin$_{MycHis}$ was a generous gift from Kate Bushby (Institute of Human Genetics, International Centre for Life, Newcastle upon Tyne, UK). The EGFP was removed with blunt religation following digestion with BsrG1 and KpnI. The cDNA is dysferlin isoform 1 (NP_003485.1), that is with exon 1, exon 17 and without exon 5a and exon 40a.). Myoferlin (NM_013451.3), Otoferlin$_{Neuronal}$ (NM_194248.2), Fer1L5 (NM_001293083.1) and Fer1L6 (NM_001039112.2) were purchased in the pCMV6 MycDDDK vector from Origene. Otoferlin$_{Ubiquitous}$ (NM_001287489.1) was derived via PCR of human brain cDNA, with primers replacing the exon 48 stop codon with an MluI restriction site. A SacII – MluI fragment bearing the C-terminal domain of Otoferlin$_{Ub}$ was subcloned into pCMV-OtoferlinNeuronal. All ferlin constructs were sub-cloned into pIRES2 EGFP for plasma membrane detection studies.

Image Processing and Statistical Analysis

All 3D-SIM images were processed using FIJI (58) and the FIJI 3D viewer plugin (59). Graphing and statistical analysis was undertaken using Graphpad Prism.

Acknowledgments

We thank Laurence Cantrill at the Westmead Research Hub Cell Imaging Facility for technical assistance with confocal microscopy, and the Children's Medical Research Institute Flow Cytometry Facility for their technical assistance. We thank Dr. Neftali Folres- Rodriguez for his Rab expression constructs and technical advice. We acknowledge the following funding bodies for supporting our work: the Australian National Health and Medical Research Council (Project Grant APP1048814 to S.T.C.; Career Development Fellowship APP1048816 to S.T.C.), the Jain Foundation (S.T.C.) and the University of Sydney for postgraduate award funding (G.R.).

References:

1. Lek A, Evesson FJ, Sutton RB, North KN, Cooper ST. Ferlins: regulators of vesicle fusion for auditory neurotransmission, receptor trafficking and membrane repair. Traffic 2012;13(2):185-194.
2. Patel P, Harris R, Geddes SM, Strehle E-M, Watson JD, Bashir R, Bushby K, Driscoll PC, Keep NH. Solution structure of the inner DysF domain of myoferlin and implications for limb girdle muscular dystrophy type 2b. J Mol Biol 2008;379(5):981-990.
3. Sula A, Cole AR, Yeats C, Orengo C, Keep NH. Crystal structures of the human Dysferlin inner DysF domain. BMC structural biology 2014;14(1):3.
4. Yan M, Rachubinski DA, Joshi S, Rachubinski RA, Subramani S. Dysferlin Domain-containing Proteins, Pex30p and Pex31p, Localized to Two Compartments, Control the Number and Size of Oleate-induced Peroxisomes in Pichia pastoris. Molecular biology of the cell 2008;19(3):885-898.
5. Lek A, Lek M, North K, Cooper S. Phylogenetic analysis of ferlin genes reveals ancient eukaryotic origins. BMC Evolutionary Biology 2010;10(1):231.
6. Sutton RB, Davletov BA, Berghuis AM, Sudhof TC, Sprang SR. Structure of the first C2 domain of synaptotagmin I: A novel Ca2+/phospholipid-binding fold. Cell 1995;80(6):929-938.
7. Xue M, Ma C, Craig TK, Rosenmund C, Rizo J. The Janus-Faced Nature of the C(2)B Domain Is Fundamental for Synaptotagmin-1 Function. Nature structural & molecular biology 2008;15(11):1160-1168.
8. Chapman ER, Davis AF. Direct Interaction of a Ca2+-binding Loop of Synaptotagmin with Lipid Bilayers. Journal of Biological Chemistry 1998;273(22):13995-14001.
9. McMahon HT, Kozlov MM, Martens S. Membrane Curvature in Synaptic Vesicle Fusion and Beyond. Cell 2010;140(5):601-605.
10. Fuson K, Rice A, Mahling R, Snow A, Nayak K, Shanbhogue P, Meyer AG, Redpath GM, Hinderliter A, Cooper ST. Alternate splicing of dysferlin C2A confers Ca 2+-dependent and Ca 2+-independent binding for membrane repair. Structure 2014;22(1):104-115.
11. Helfmann S, Neumann P, Tittmann K, Moser T, Ficner R, Reisinger E. The Crystal Structure of the C2A Domain of Otoferlin Reveals an Unconventional Top Loop Region. J Mol Biol 2011;406(3):479-490.
12. Abdullah N, Padmanarayana M, Marty NJ, Johnson CP. Quantitation of the calcium and membrane binding properties of the c2 domains of dysferlin. Biophysical journal 2014;106(2):382-389.
13. Therrien C, Di Fulvio S, Pickles S, Sinnreich M. Characterization of Lipid Binding Specificities of Dysferlin C2 Domains Reveals Novel Interactions with Phosphoinositides†. Biochemistry 2009;48(11):2377-2384.
14. Padmanarayana M, Hams N, Speight LC, Petersson EJ, Mehl RA, Johnson CP. Characterization of the Lipid Binding Properties of Otoferlin Reveals Specific Interactions between PI(4,5)P2 and the C2C and C2F Domains. Biochemistry 2014;53(30):5023-5033.
15. Liu J, Aoki M, Illa I, Wu C, Fardeau M, Angelini C, Serrano C, Urtizberea JA, Hentati F, Hamida MB, Bohlega S, Culper EJ, Amato AA, Bossie K, Oeltjen J*, et al.* Dysferlin, a novel skeletal muscle gene, is mutated in Miyoshi myopathy and limb girdle muscular dystrophy. Nat Genet 1998;20(1):31-36.
16. Bashir R, Britton S, Strachan T, Keers S, Vafiadaki E, Lako M, Richard I, Marchand S, Bourg N, Argov Z, Sadeh M, Mahjneh I, Marconi G, Passos-Bueno MR, Moreira EdS*, et al.* A gene related to Caenorhabditis elegans spermatogenesis factor fer-1 is mutated in limb-girdle muscular dystrophy type 2B. Nat Genet 1998;20(1):37-42.
17. Bansal D, Miyake K, Vogel SS, Groh S, Chen C-C, Williamson R, McNeil PL, Campbell KP. Defective membrane repair in dysferlin-deficient muscular dystrophy. Nature 2003;423(6936):168-172.
18. Steinhardt R, Bi G, Alderton J. Cell membrane resealing by a vesicular mechanism similar to neurotransmitter release. Science 1994;263(5145):390-393.
19. Lek A, Evesson FJ, Lemckert FA, Redpath GMI, Lueders A-K, Turnbull L, Whitchurch CB, North KN, Cooper ST. Calpains, Cleaved Mini-DysferlinC72, and L-Type Channels Underpin Calcium-Dependent Muscle Membrane Repair. The Journal of Neuroscience 2013;33(12):5085-5094.
20. Roostalu U, Strähle U. In Vivo Imaging of Molecular Interactions at Damaged Sarcolemma. Developmental Cell 2012;22(3):515-529.
21. Yasunaga Si, Grati Mh, Cohen-Salmon M, El-Amraoui A, Mustapha M, Salem N, El-Zir E, Loiselet J, Petit C. A mutation in OTOF, encoding otoferlin, a FER-1-like protein, causes DFNB9, a nonsyndromic form of deafness. Nat Genet 1999;21(4):363-369.
22. Yasunaga Si, Grati Mh, Chardenoux S, Smith TN, Friedman TB, Lalwani AK, Wilcox ER, Petit C. OTOF Encodes Multiple Long and Short Isoforms: Genetic Evidence That the Long Ones Underlie Recessive Deafness DFNB9. The American Journal of Human Genetics 2000;67(3):591-600.

23. Roux I, Safieddine S, Nouvian R, Grati Mh, Simmler M-C, Bahloul A, Perfettini I, Le Gall M, Rostaing P, Hamard G, Triller A, Avan P, Moser T, Petit C. Otoferlin, Defective in a Human Deafness Form, Is Essential for Exocytosis at the Auditory Ribbon Synapse. Cell 2006;127(2):277-289.
24. Turtoi A, Blomme A, Bellahcène A, Gilles C, Hennequière V, Peixoto P, Bianchi E, Noel A, De Pauw E, Lifrange E, Delvenne P, Castronovo V. Myoferlin Is a Key Regulator of EGFR Activity in Breast Cancer. Cancer Research 2013;73(17):5438-5448.
25. Volakis LI, Li R, Ackerman WEIV, Mihai C, Bechel M, Summerfield TL, Ahn CS, Powell HM, Zielinski R, Rosol TJ, Ghadiali SN, Kniss DA. Loss of Myoferlin Redirects Breast Cancer Cell Motility towards Collective Migration. PLoS ONE 2014;9(2):e86110.
26. Amatschek S, Koenig U, Auer H, Steinlein P, Pacher M, Gruenfelder A, Dekan G, Vogl S, Kubista E, Heider K-H, Stratowa C, Schreiber M, Sommergruber W. Tissue-Wide Expression Profiling Using cDNA Subtraction and Microarrays to Identify Tumor-Specific Genes. Cancer Research 2004;64(3):844-856.
27. Leung C, Yu C, Lin MI, Tognon C, Bernatchez P. Expression of Myoferlin in Human and Murine Carcinoma Tumors: Role in Membrane Repair, Cell Proliferation, and Tumorigenesis. The American Journal of Pathology 2013;182(5):1900-1909.
28. Wang W-S, Liu X-H, Liu L-X, Lou W-H, Jin D-Y, Yang P-Y, Wang X-L. iTRAQ-based quantitative proteomics reveals myoferlin as a novel prognostic predictor in pancreatic adenocarcinoma. Journal of Proteomics 2013;91(0):453-465.
29. Davis DB, Delmonte AJ, Ly CT, McNally EM. Myoferlin, a candidate gene and potential modifier of muscular dystrophy. Human Molecular Genetics 2000;9(2):217-226.
30. Demonbreun AR, Lapidos KA, Heretis K, Levin S, Dale R, Pytel P, Svensson EC, McNally EM. Myoferlin regulation by NFAT in muscle injury, regeneration and repair. Journal of Cell Science 2010;123(14):2413-2422.
31. Song H, Sun W, Ye G, Ding X, Liu Z, Zhang S, Xia T, Xiao B, Xi Y, Guo J. Long non-coding RNA expression profile in human gastric cancer and its clinical significances. Journal of Translational Medicine 2013;11(1):225.
32. Glover LE, Newton K, Krishnan G, Bronson R, Boyle A, Krivickas LS, Brown RH. Dysferlin overexpression in skeletal muscle produces a progressive myopathy. Annals of Neurology 2010;67(3):384-393.
33. Hudson AW, Birnbaum MJ. Identification of a nonneuronal isoform of synaptotagmin. Proceedings of the National Academy of Sciences 1995;92(13):5895-5899.
34. Gauthier BR, Wollheim CB. Synaptotagmins bind calcium to release insulin; 2008.
35. Südhof TC. Synaptotagmins: Why So Many? Journal of Biological Chemistry 2002;277(10):7629-7632.
36. Nishiki T-i, Augustine GJ. Synaptotagmin I synchronizes transmitter release in mouse hippocampal neurons. The Journal of Neuroscience 2004;24(27):6127-6132.
37. Shin O-H, Xu J, Rizo J, Südhof TC. Differential but convergent functions of Ca2+ binding to synaptotagmin-1 C2 domains mediate neurotransmitter release. Proceedings of the National Academy of Sciences 2009;106(38):16469-16474.
38. Gut A, Kiraly CE, Fukuda M, Mikoshiba K, Wollheim CB, Lang J. Expression and localisation of synaptotagmin isoforms in endocrine (β)-cells: their function in insulin exocytosis. Journal of Cell Science 2001;114(9):1709-1716.
39. Gustavsson N, Wei S-H, Hoang DN, Lao Y, Zhang Q, Radda GK, Rorsman P, Südhof TC, Han W. Synaptotagmin-7 is a principal Ca(2+) sensor for Ca(2+)-induced glucagon exocytosis in pancreas. The Journal of Physiology 2009;587(Pt 6):1169-1178.
40. Gustafsson MGL, Shao L, Carlton PM, Wang CJR, Golubovskaya IN, Cande WZ, Agard DA, Sedat JW. Three-Dimensional Resolution Doubling in Wide-Field Fluorescence Microscopy by Structured Illumination. Biophysical journal 2008;94(12):4957-4970.
41. Evesson FJ, Peat RA, Lek A, Brilot F, Lo HP, Dale RC, Parton RG, North KN, Cooper ST. Reduced Plasma Membrane Expression of Dysferlin Mutants Is Attributed to Accelerated Endocytosis via a Syntaxin-4-associated Pathway. Journal of Biological Chemistry 2010;285(37):28529-28539.
42. Bernatchez PN, Sharma A, Kodaman P, Sessa WC. Myoferlin is critical for endocytosis in endothelial cells. American Journal of Physiology - Cell Physiology 2009;297(3):C484-C492.
43. Reaves B, Banting G. Perturbation of the morphology of the trans-Golgi network following Brefeldin A treatment: redistribution of a TGN-specific integral membrane protein, TGN38. J Cell Biol 1992;116(1):85-94.
44. Demonbreun AR, Fahrenbach JP, Deveaux K, Earley JU, Pytel P, McNally EM. Impaired muscle growth and response to insulin-like growth factor 1 in dysferlin-mediated muscular dystrophy. Human Molecular Genetics 2011;20(4):779-789.

45. Pangrsic T, Lasarow L, Reuter K, Takago H, Schwander M, Riedel D, Frank T, Tarantino LM, Bailey JS, Strenzke N, Brose N, Muller U, Reisinger E, Moser T. Hearing requires otoferlin-dependent efficient replenishment of synaptic vesicles in hair cells. Nat Neurosci 2010;13(7):869-876.
46. Choi BY, Ahmed ZM, Riazuddin S, Bhinder M, Shahzad M, Husnain T, Griffith A, Friedman T. Identities and frequencies of mutations of the otoferlin gene (OTOF) causing DFNB9 deafness in Pakistan. Clinical genetics 2009;75(3):237-243.
47. Schug N, Braig C, Zimmermann U, Engel J, Winter H, Ruth P, Blin N, Pfister M, Kalbacher H, Knipper M. Differential expression of otoferlin in brain, vestibular system, immature and mature cochlea of the rat. European Journal of Neuroscience 2006;24(12):3372-3380.
48. Heidrych P, Zimmermann U, Breß A, Pusch CM, Ruth P, Pfister M, Knipper M, Blin N. Rab8b GTPase, a protein transport regulator, is an interacting partner of otoferlin, defective in a human autosomal recessive deafness form. Human Molecular Genetics 2008;17(23):3814-3821.
49. Vincent PF, Bouleau Y, Safieddine S, Petit C, Dulon D. Exocytotic machineries of vestibular type I and cochlear ribbon synapses display similar intrinsic otoferlin-dependent Ca2+ sensitivity but a different coupling to Ca2+ channels. The Journal of Neuroscience 2014;34(33):10853-10869.
50. Leung C, Shaheen F, Bernatchez P, Hackett T-L. Expression of Myoferlin in Human Airway Epithelium and Its Role in Cell Adhesion and Zonula Occludens-1 Expression. PLoS ONE 2012;7(7):e40478.
51. Doherty KR, Cave A, Davis DB, Delmonte AJ, Posey A, Earley JU, Hadhazy M, McNally EM. Normal myoblast fusion requires myoferlin. Development 2005;132(24):5565-5575.
52. Doherty KR, Demonbreun AR, Wallace GQ, Cave A, Posey AD, Heretis K, Pytel P, McNally EM. The endocytic recycling protein EHD2 interacts with myoferlin to regulate myoblast fusion. Journal of Biological Chemistry 2008;283(29):20252-20260.
53. Posey AD, Pytel P, Gardikiotes K, Demonbreun AR, Rainey M, George M, Band H, McNally EM. Endocytic Recycling Proteins EHD1 and EHD2 Interact with Fer-1-like-5 (Fer1L5) and Mediate Myoblast Fusion. Journal of Biological Chemistry 2011;286(9):7379-7388.
54. Revelo NH, Kamin D, Truckenbrodt S, Wong AB, Reuter-Jessen K, Reisinger E, Moser T, Rizzoli SO. A new probe for super-resolution imaging of membranes elucidates trafficking pathways. J Cell Biol 2014;205(4):591-606.
55. Lenhart KC, Becherer AL, Li J, Xiao X, McNally EM, Mack CP, Taylor JM. GRAF1 promotes ferlin-dependent myoblast fusion. Developmental Biology 2014;393(2):298-311.
56. Posey Jr AD, Swanson KE, Alvarez MG, Krishnan S, Earley JU, Band H, Pytel P, McNally EM, Demonbreun AR. EHD1 mediates vesicle trafficking required for normal muscle growth and transverse tubule development. Developmental Biology 2014;387(2):179-190.
57. Strauss MP, Liew ATF, Turnbull L, Whitchurch CB, Monahan LG, Harry EJ. 3D-SIM Super Resolution Microscopy Reveals a Bead-Like Arrangement for FtsZ and the Division Machinery: Implications for Triggering Cytokinesis. PLoS Biol 2012;10(9):e1001389.
58. Schindelin J, Arganda-Carreras I, Frise E, Kaynig V, Longair M, Pietzsch T, Preibisch S, Rueden C, Saalfeld S, Schmid B, Tinevez J-Y, White DJ, Hartenstein V, Eliceiri K, Tomancak P*, et al.* Fiji: an open-source platform for biological-image analysis. Nat Meth 2012;9(7):676-682.
59. Schmid B, Schindelin J, Cardona A, Longair M, Heisenberg M. A high-level 3D visualization API for Java and ImageJ. BMC Bioinformatics 2010;11(1):274.

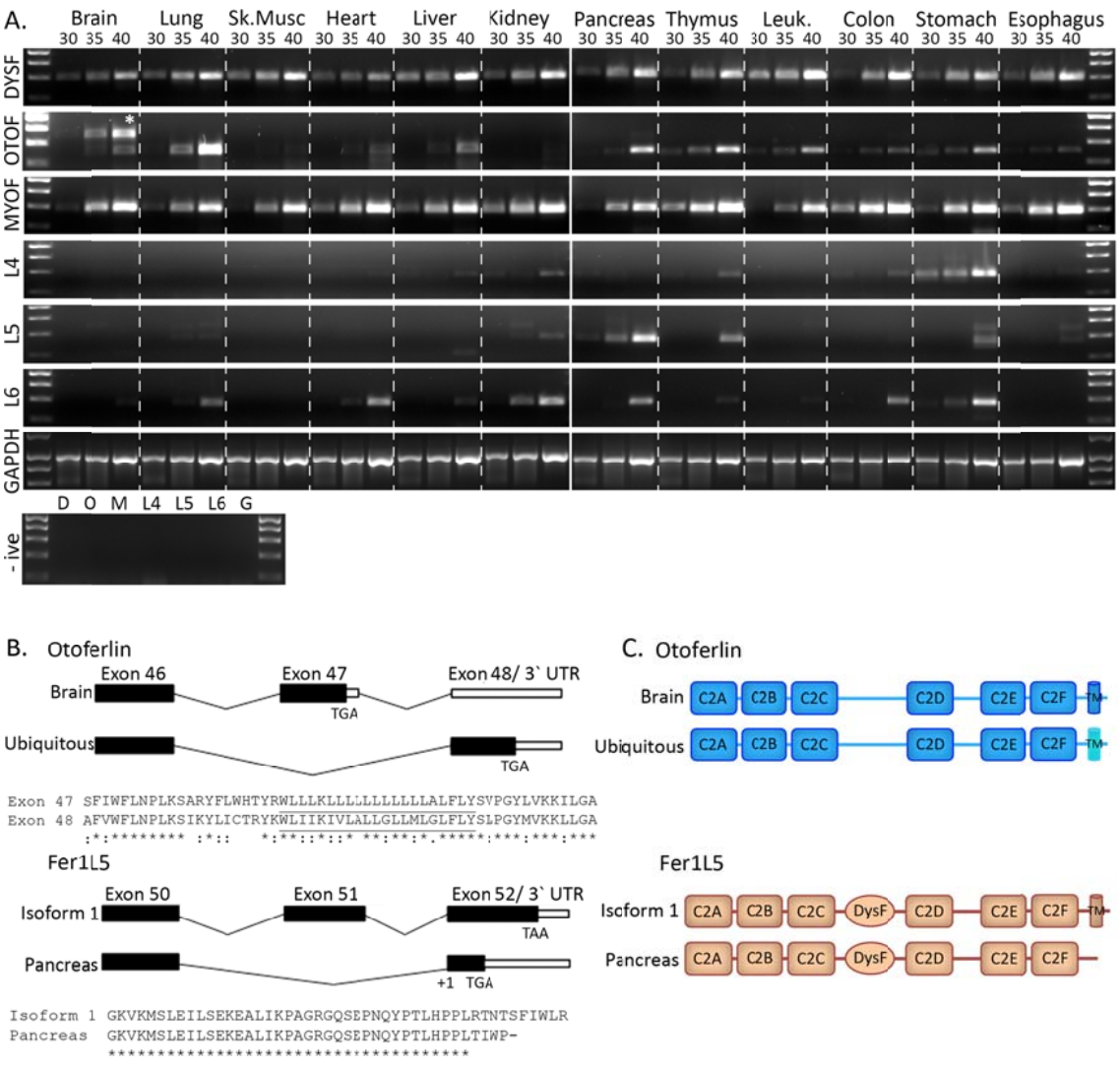

Figure 1: Expression of ferlins in human cDNA panels. A- Each ferlin was amplified from human cDNA panels (Clontech MTC Panel I, Immune Panel and Gut Panel) for 30, 35 and 40 cycles. GAPDH was amplified as a positive control, and water only negative controls included for each primer set for 40 cycles. Gels are flanked with Hyperladder I (800, 600, 400 and 200bp bands are present). **B-** Schematic of alternate-splicing events affecting the transmembrane domains of otoferlin and Fer1L5, with the translated protein sequences for each isoform below. Alignments were performed with ClustalW. The predicted transmembrane domains for each otoferlin isoform are underlined. **C-** Schematic of otoferlin and Fer1L5 protein structures demonstrating how alternate-splicing of otoferlin and Fer1L5 affect the transmembrane domains.

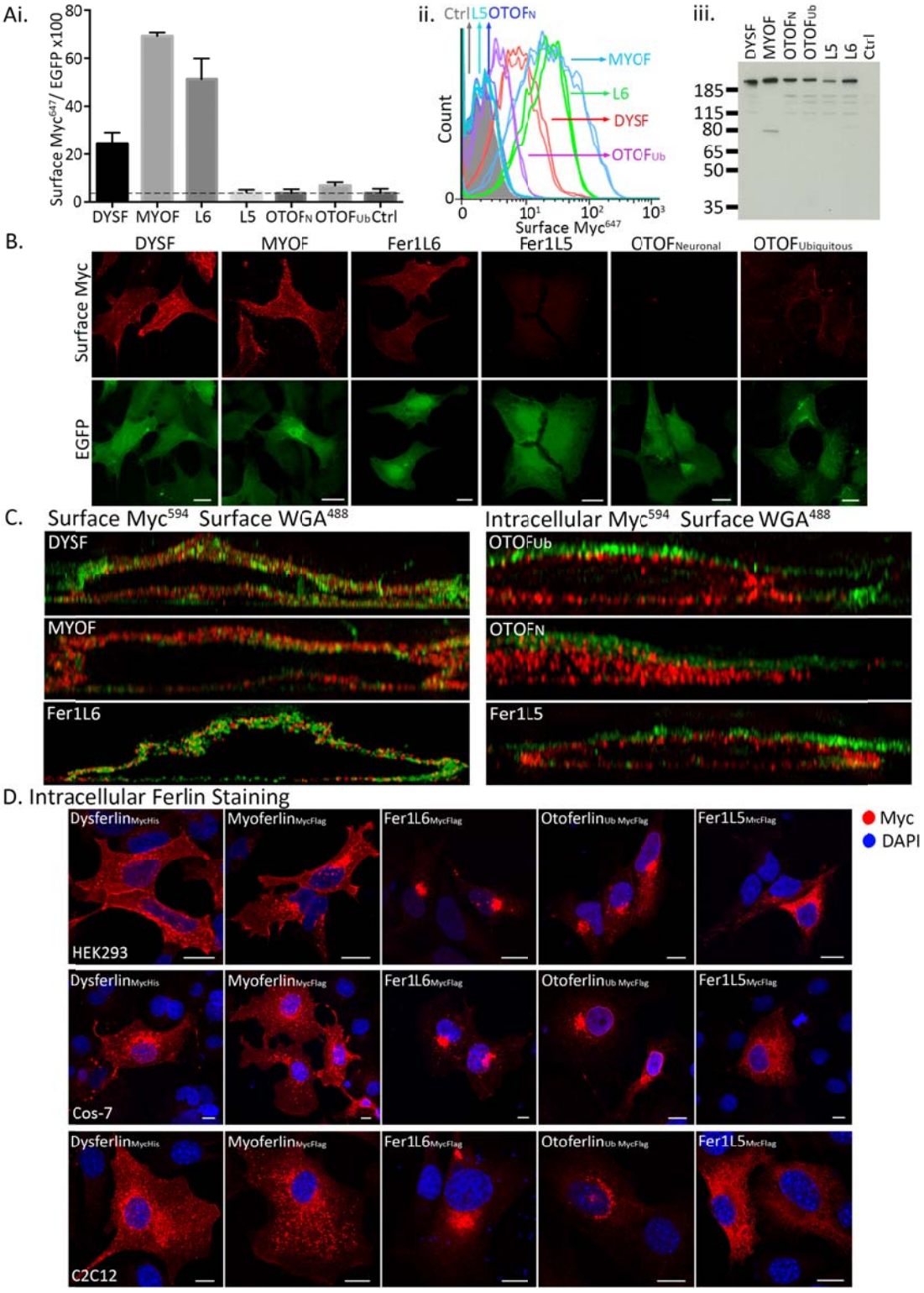

Figure 2: Dysferlin, myoferlin and Fer1L6 are plasma membrane ferlins. A *i)* Histogram showing the plasma membrane expression of each ferlin in transfected HEK293 cells quantified by flow cytometry. HEK293 cells were transfected with pIRES constructs expressing each mammalian ferlin bearing a luminal Myc tag. The internal ribosome entry site (IRES) separately co-translates EGFP and the ferlin from the same mRNA. Live cells were dissociated from the plate with Versene and labelled with anti-Myc^{Alexa647} at 8°C for 90 minutes in blocking solution (HBSS with 10% FBS). Live cells were gated by exclusion of propidium iodide and surface bound anti-Myc^{Alexa647} is plotted relative to the EGFP fluorescence for each sample. The dashed line indicates background non-specific staining of vector-only controls. Error bars represent S.D. of three experimental replicates performed in duplicate. ***ii)*** The normal distribution of surface anti-Myc^{Alexa647} labeling observed in duplicate samples from a single experiment. The transfection efficiency calculated by the GFP-positive gate with flow cytomtery was: Dysf – 25.5%, Myof – 14.6%, Fer1L5 – 25.5%, Fer1L6 – 6.69% and OtofN – 11.7, %, OtofUb – 10.2%, control pIRES vector – 7.38%. ***iii)*** Western blot of samples probed with anti-Myc from the same experiment confirming each ferlin is expressed. 10 µg of transfected HEK293 RIPA lysate, as determined by BCA assay, was separated by SDS-PAGE and transferred onto PVDF membrane. **B-** Additional cells from 'A' were replated onto coverslips and subject to surface labeling with anti-Myc (Alexa^{555}). Microscopy shows dysferlin, myoferlin and Fer1L6 are abundantly expressed at the cell surface. Otoferlin$_{Ub}$ is detectable at low levels on the cell surface, whereas the neuronal isoform of otoferlin$_N$ and Fer1L5 are not present at levels above background at the plasma membrane, consistent with flow cytometry results. Images were captured using a Leica SP5 confocal. Scale bars: 10 µM. **C)** 3D-structured illumination microscopy (3D-SIM) of live surface-stained cells (Left; DYSF, MYOF, Fer1L6), or total intracellular staining of fixed and permeabilised cells (Right; OTOFUb, OTOFN and Fer1L5). Images shown are single y-z planes with the apical membrane above and the basolateral membrane below. **D)** Confocal microscopy of total intracellular labeling of fixed and permeabilised HEK293 (top panel), Cos-7 (middle panel) and C2C12 (bottom panel) cells transfected with each ferlin expression construct reveals a unique subcellular localization for each ferlin. Confocal images are presented as single Z-sections.

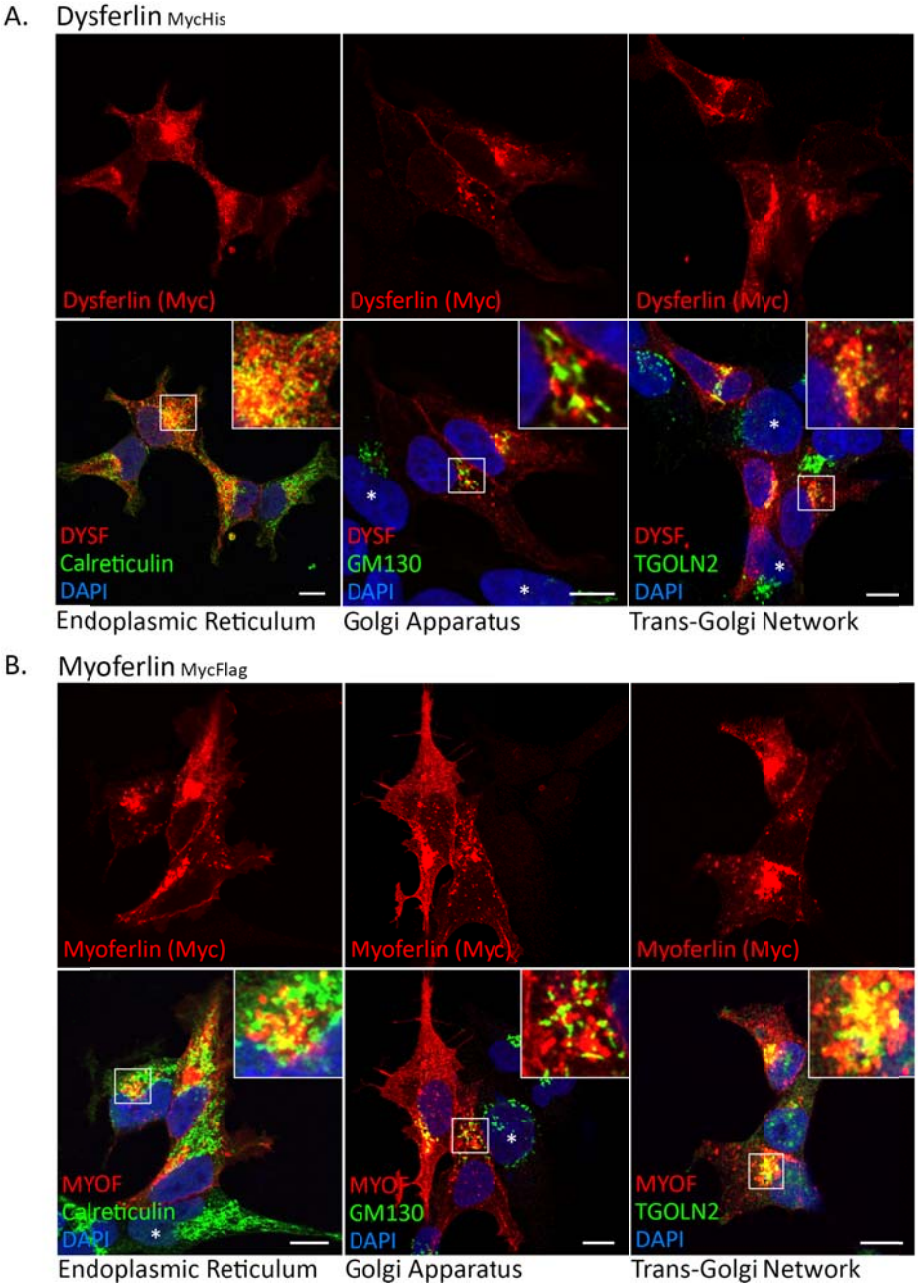

Figure 3: Total intracellular labeling for dysferlin$_{MycHis}$ (A) and myoferlin$_{MycFlag}$ (B) with secretory pathway markers. HEK293 cells were transfected with dysferlin and myoferlin expression constructs (lacking EGFP) then re-plated onto coverslips overnight. Cells were fixed, permeabilised and labeled with anti-Myc (Alexa^{594} OR Alexa^{488} false coloured red) and co-stained with markers for the endoplasmic reticulum (calreticulin), cis-Golgi (GM130) or trans-Golgi (TGOLN2) (Alexa^{488} OR Alexa^{594} false coloured green). Nuclei were labeled with DAPI (blue). Scale bars: 10 μM. Untransfected cells within imaged fields are labeled with an asterisk, demonstrating the specificity of labeling by the anti-Myc antibody.

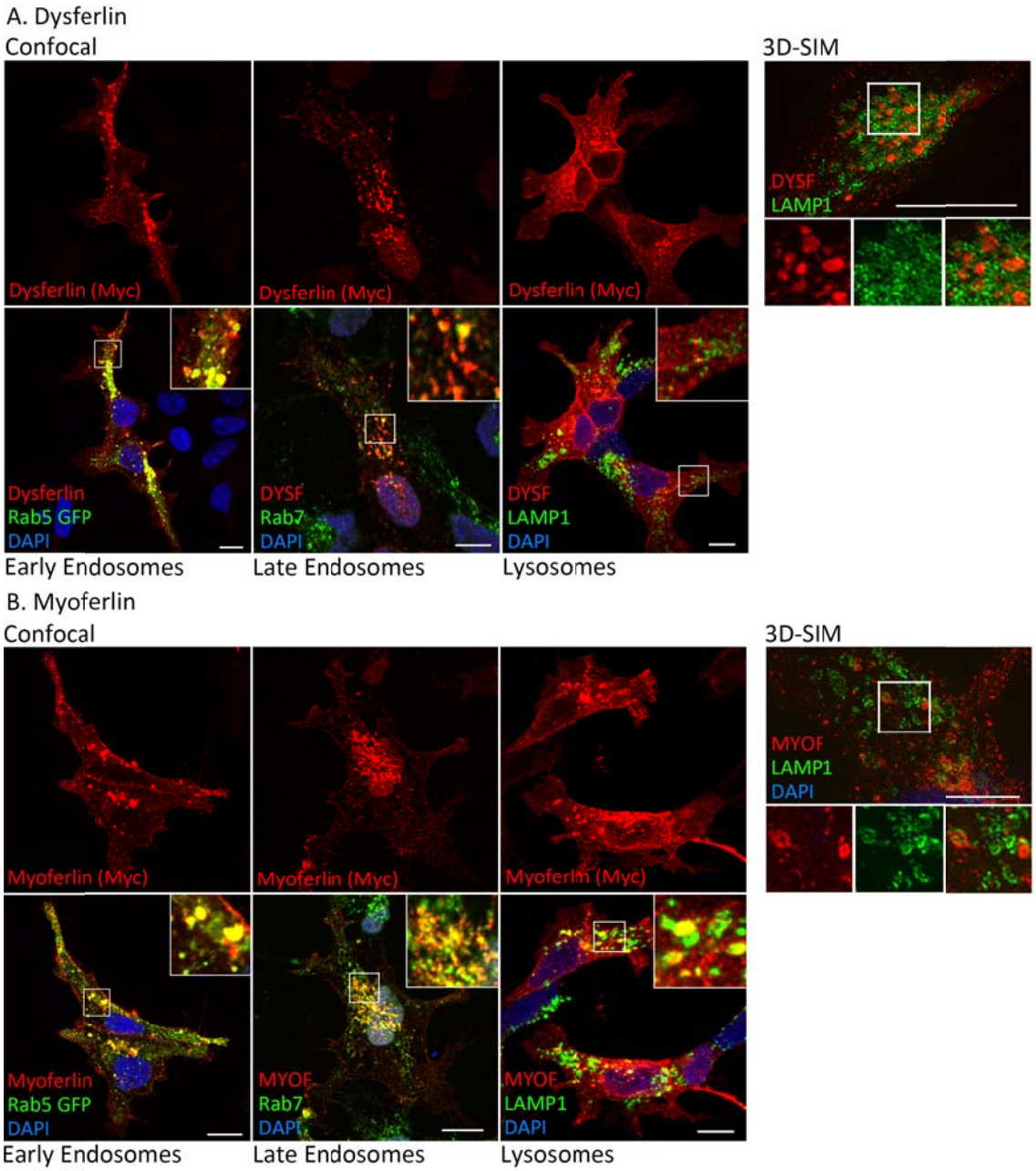

Figure 4: Total intracellular labeling of dysferlin$_{MycHis}$ (A) and myoferlin$_{MycFlag}$ (B) with endo-lysosomal pathway markers. HEK293 cells were transfected with either dysferlin or myoferlin expression constructs (lacking EGFP) and replated onto coverslips overnight. For detection of early endosomes, cells were co-transfected with Rab5-EGFP and dysferlin/myoferlin. Dysferlin and myoferlin were detected with anti-Myc (red), and co-labeled with markers for early endosomes (in Rab5-EGFP co-transfected cells, anti-EGFP), late endosomes (Rab7) or lysosomes (LAMP1) (green) to delineate the endo-lysosomal pathway. Scale bars: 10 µM.

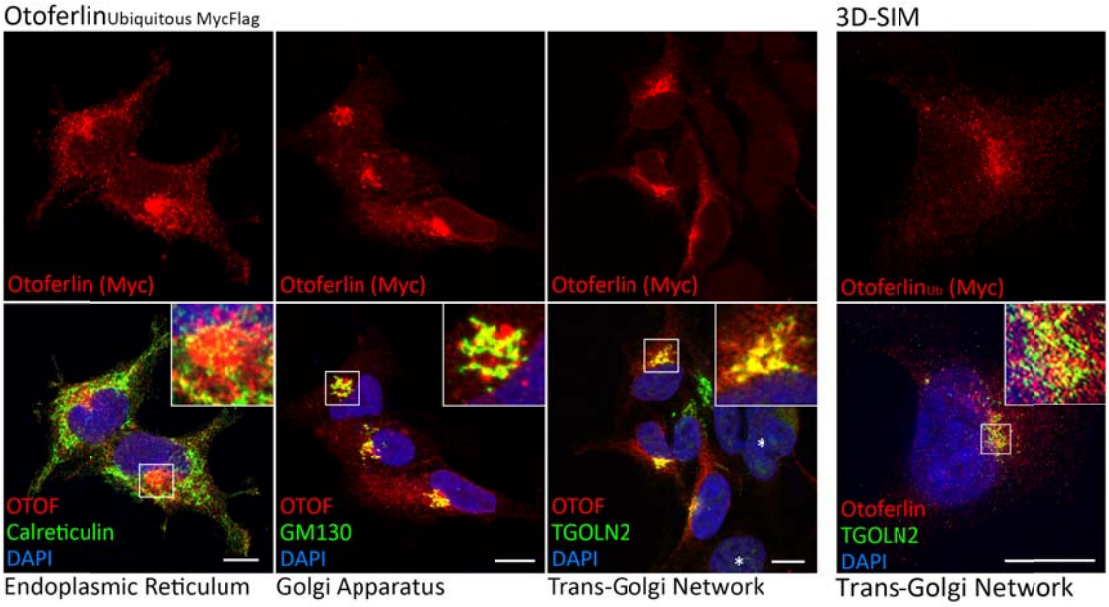

Figure 5: Total intracellular labeling of otoferlin-Ubiquitous $_{MycFlag}$ with secretory pathway markers. HEK293 cells were transfected with *ubiquitous* pCMV6-otoferlin$_{MycFlag}$ (lacking EGFP) and re-plated onto coverslips overnight. Otoferlin was detected with anti-Myc (red) and co-labeled with markers for the endoplasmic reticulum (calreticulin), cis-Golgi (GM130) or trans-Golgi (TGOLN2) (green). Nuclei were labeled with DAPI (blue). Images were captured on a Leica SP5 confocal (single z-sections presented) or DeltaVision OMX 3D-SIM (indicated right panel, z-projection). Scale bars: 10 μM. Untransfected cells are labeled with an asterisk.

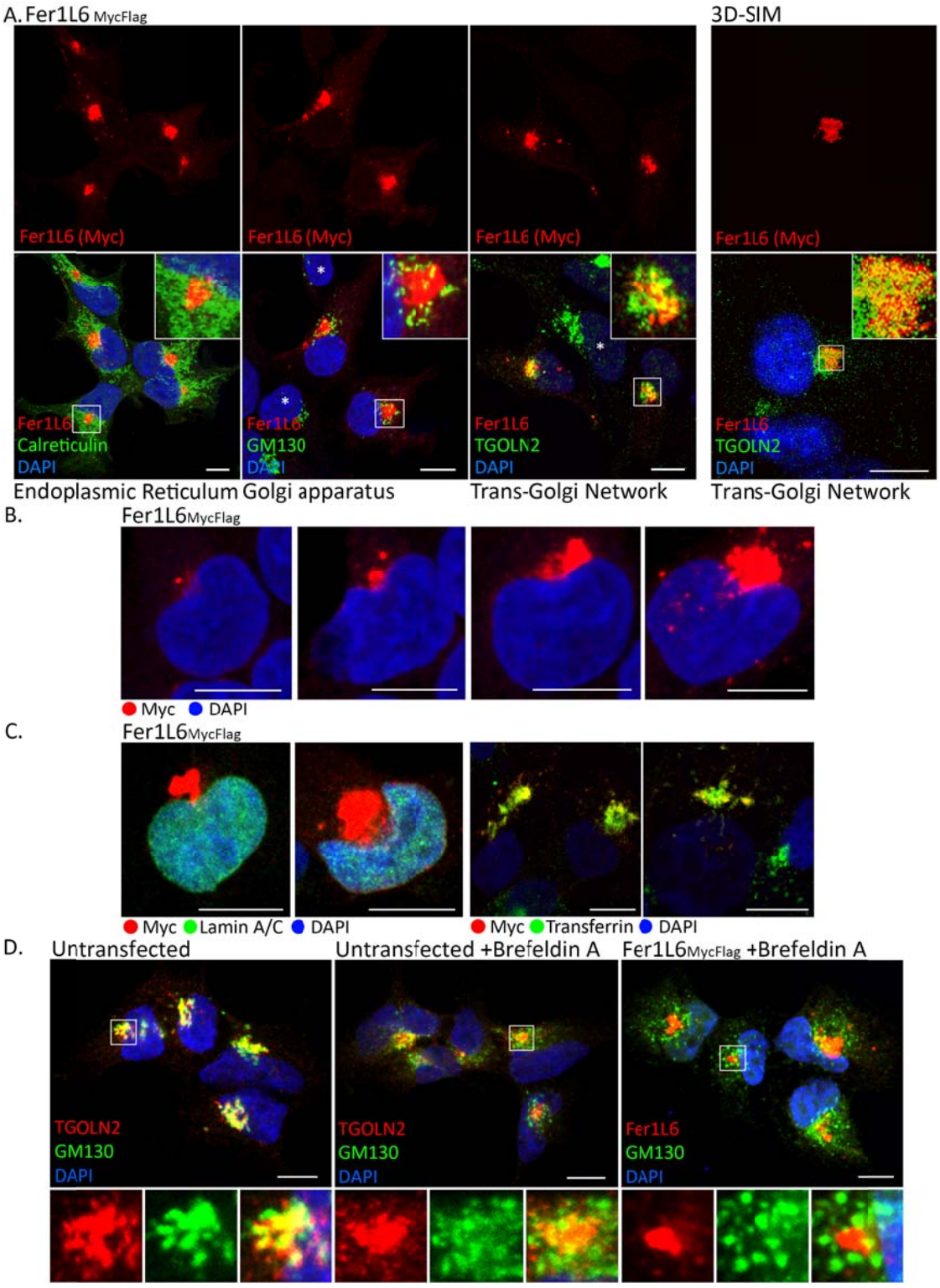

Figure 6: Fer1L6$_{MycFlag}$ localises to a brefeldin-A resistant, transferrin^{594}-positive recycling compartment. HEK293 cells were transfected with Fer1L6$_{MycFlag}$-pCMV6 (lacking EGFP) then re-plated onto coverslips overnight. Fer1L6 was detected in fixed, permeabilised cells with anti-Myc (red). Nuclei were labeled with DAPI (blue). **A-** Cells were co-labeled with markers for the endoplasmic reticulum (calreticulin), cis-Golgi (GM130) or trans-Golgi (TGOLN2) (green). Images were captured on a Leica SP5 confocal (single z-sections presented) or DeltaVision OMX 3D-SIM (indicated right panel, z-projection). **B-** Representative confocal images portraying how increasing levels of Fer1L6 expression (anti-Myc, red) increasingly labels a perinuclear compartment that

deforms the nucleus in highly expressing cells. **C-** Fer1L6, detected with anti-Myc, co-localises with endocytosed transferrin^{594} (false colored green, right panel) and labels a compartment separate to the nuclear envelope detected with lamin A/C (left panels). The intensity of Fer1L6 labeling of the perinuclear compartment requires very low laser power for imaging and can preclude visibility of the plasma membrane. **D-** HEK293 cells were incubated in the presence or absence of 5 µg.mL^{-1} brefeldin-A for 90 minutes at 37°C (as indicated). Cells were fixed, permeabilised and labeled with anti-Myc (Fer1L6, red) and GM130 or TGOLN2 left and middle panels, green). Images were captured on a Leica SP5 confocal (single Z-sections presented). Scale bar: 10 µM. Untransfected cells are labeled with an asterisk.

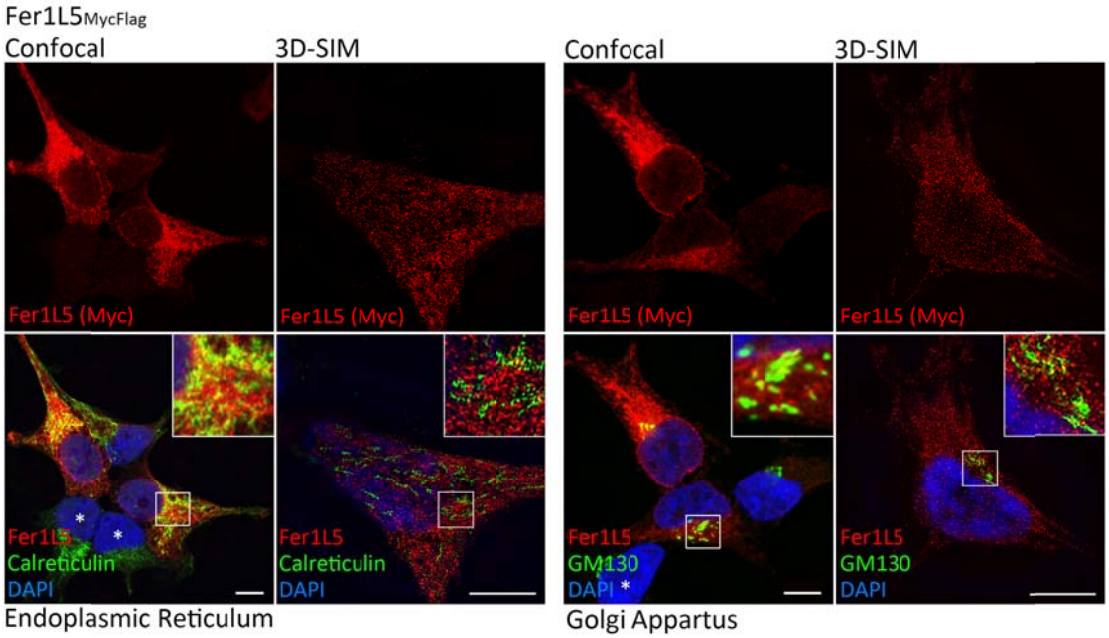

Figure 7: Fer1L5 does not co-localise with markers of the secretory pathway with total intracellular labeling. HEK293 cells transfected with Fer1L5$_{MycFlag}$-pCMV6 (lacking EGFP) were re-plated onto coverslips overnight. Fer1L5 was detected with anti-Myc (red) and co-labeled for the ER (calreticulin) or the Golgi apparatus (GM130) (green). Nuclei were labeled with DAPI (blue). Images were captured on a Leica SP5 confocal or DeltaVision OMX 3D-SIM as indicated (single Z-sections presented). Scale bar: 10 µM. Untransfected cells are labeled with an asterisk.

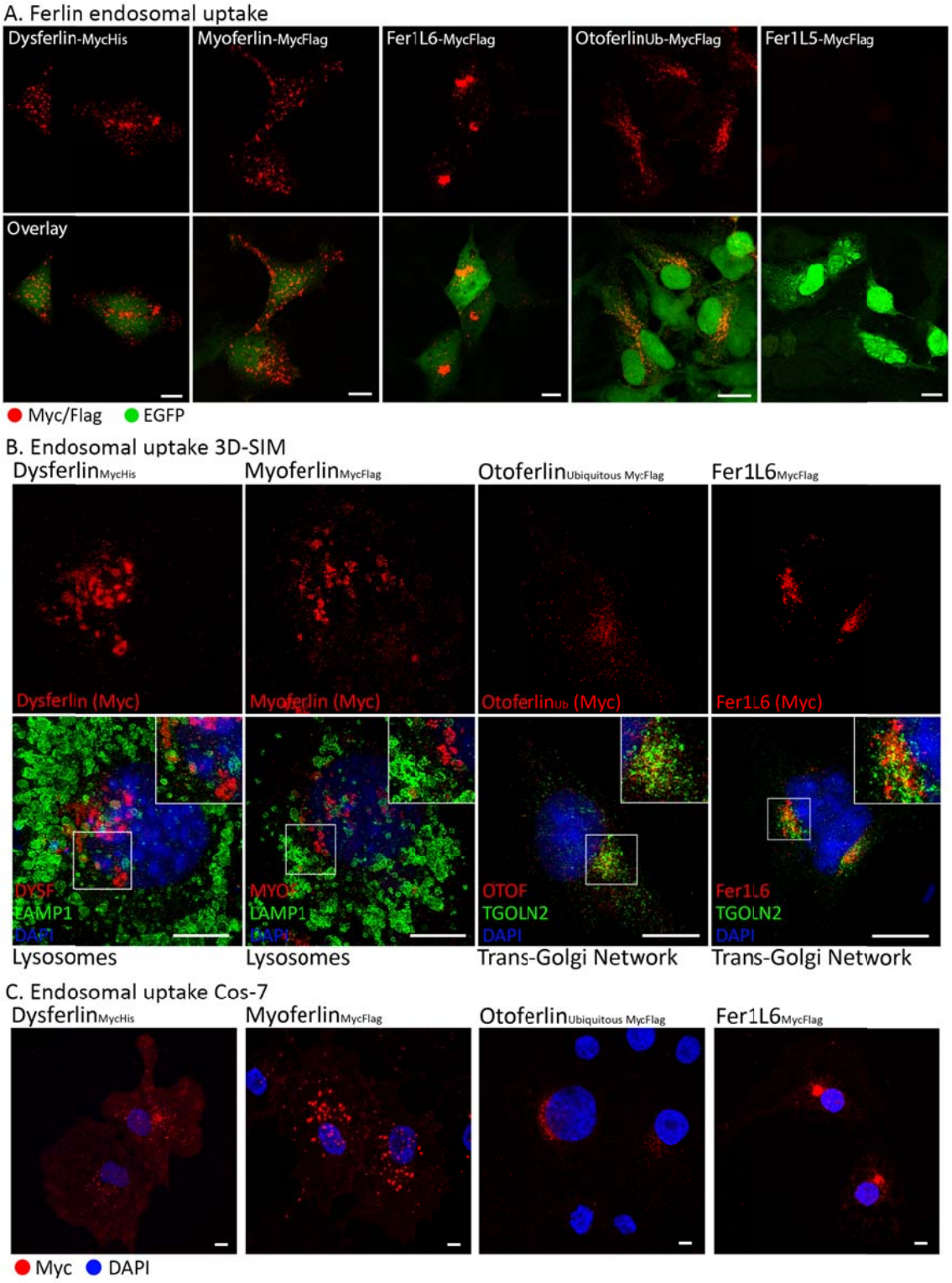

Figure 8: Retrograde antibody labeling of ferlin endocytic pathways reveals lysosomal (dysferlin and myoferlin) or trans-Golgi (otoferlin, Fer1L6) endocytosis. To label ferlin endocytic pathways using retrograde antibody trafficking, cells were incubated with anti-Myc in replacement media at 37°C for up to 90 minutes (as indicated). Surface bound anti-Myc was removed by washing coverslips in 0.5 M pH 2.2 glycine, allowing specific detection of endocytosed anti-Myc. Cells were then fixed with ice-cold PFA, permeabilised and endocytosed anti-Myc detected with anti-rabbit Alexa^{594} (or Alexa^{488} false coloured red). **A-** Transfected HEK293 cells subject to endocytic tracing with anti-Myc uptake for 90 minutes. Images were captured on a Leica SP5 confocal. Scale

bars 10 μM. **B-** Transfected C2C12 (dysferlin$_{MycHis}$ or myoferlin$_{MycFlag}$) or HEK293 cells (Fer1L6$_{MycFlag}$ and otoferlin-Ub$_{MycFlag}$) were labeled at 37°C by anti-Myc uptake for 30 minutes. Cells were acid washed, fixed and permeabilised then co-labeled for lysosomes (LAMP1, Alexa^{488}) or the trans-Golgi network (TGOLN2, Alexa^{594} false coloured green). Images were captured on a DeltaVision OMX 3D-SIM (Z-projections presented). Scale bars 10 μM. *Note*: experiments were performed for all constructs in both cell lines, with representative images presented. **C-** Transfected Cos-7 cells labeled by anti-Myc uptake at 37°C for 30 minutes. Following acid wash, fixation and permeabilisation, internalized anti-Myc was detected with anti-rabbit Alexa^{594}. Scale bars 10μM.

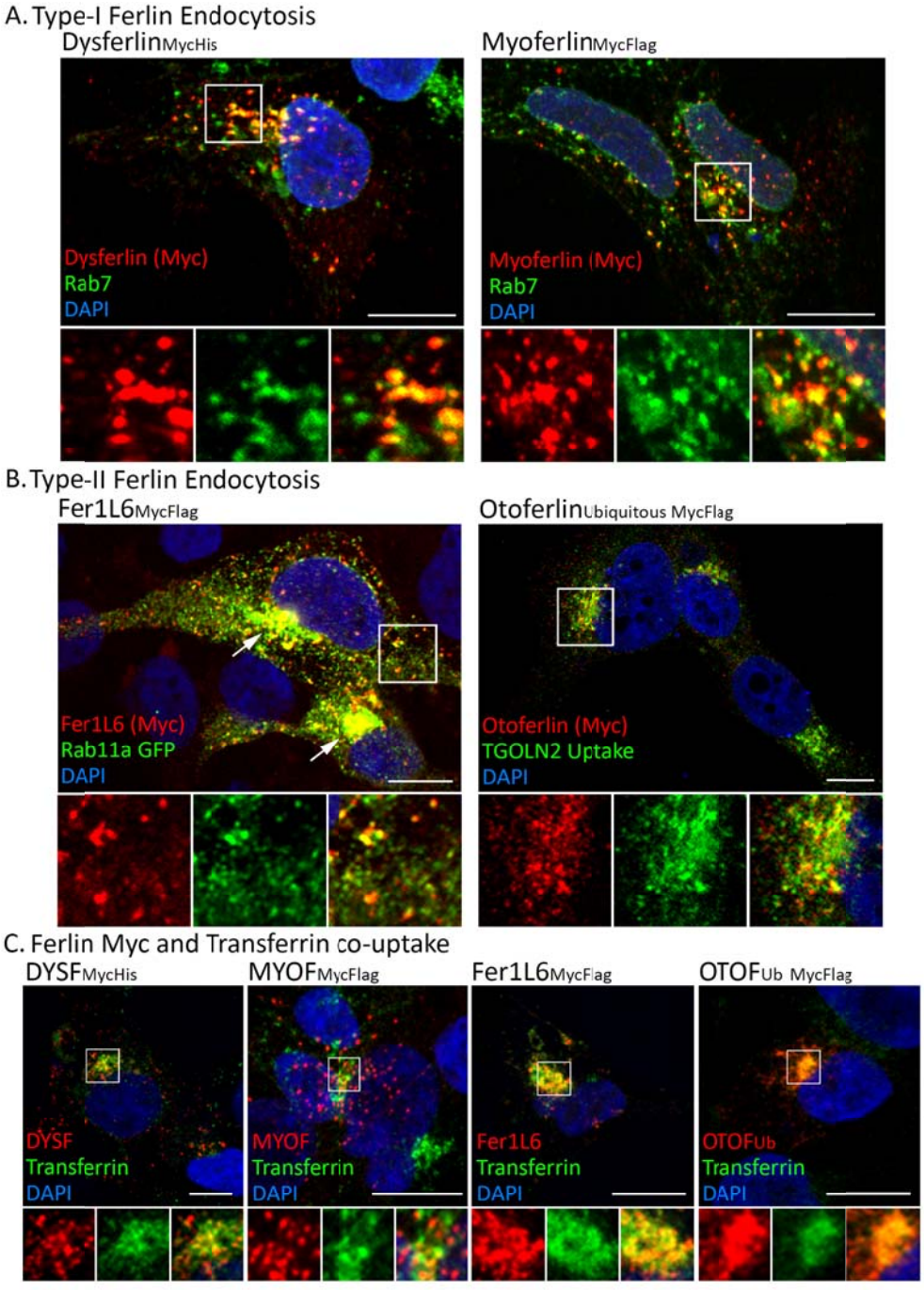

Figure 9: Dysferlin and myoferlin endocytose via late endosomes, Fer1L6 on recycling endosomes and otoferlin endocytosis is independent of TGOLN2. A- HEK293 cells were transfected with dysferlin$_{MycHis}$ or myoferlin$_{MycFlag}$ expression constructs (lacking EGFP) and incubated with anti-Myc in media at 37°C for 90

minutes to label ferlin endocytic trafficking. Following acid wash, fixation and permeabilisation, endocytosed anti-Myc was detected with Alexa^{488} (false coloured red) and late endosomes with anti-Rab7 (Alexa^{594}, false coloured green). **B- Left:** HEK293 cells co-transfected with Fer1L6$_{MycFlag}$ and Rab11a-EGFP were subject to antibody uptake with anti-Myc in media at 37°C 10 minutes. Endocytosed anti-Myc was detected with anti-rabbit Alexa^{594} and Rab11a with anti-EGFP (Alexa^{488}). **Right:** HEK293 cells transfected with otoferlin-Ub$_{MycFlag}$ were incubated with anti-Myc and anti-TGOLN2 together in media at 37°C for 90 minutes to label both otoferlin and TGOLN2 endocytic pathways. Endocytosed anti-Myc and anti-TGOLN2 were detected with Alexa^{488} (false coloured red) and Alexa^{594} (false coloured green) respectively. All images were captured on a Leica SP5 confocal (single z-sections presented). **C-** Anti-Myc andtransferrin^{594} (false coloured green) were applied to the cell media at 37°C for 30 minutes to label endocytic uptake. Following acid wash, fixation and permeabilisation anti-Myc was detected with anti-rabbit^{488} (false coloured green). Scale bars: 10 μM.

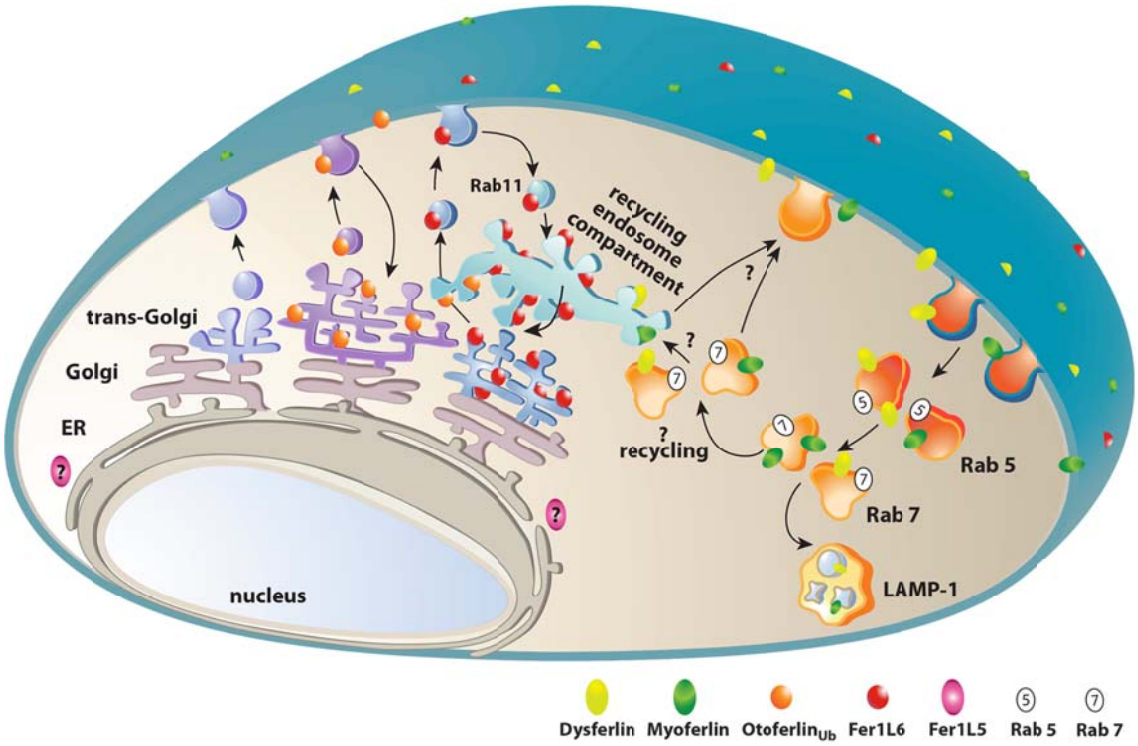

Figure 10: Schematic diagram depicting the intracellular localization and endocytic trafficking of the ferlins. Dysferlin (yellow) and myoferlin (green) abundantly label the plasma membrane and transit through the endo-lysosomal pathway accumulating in Rab7-positive late endosomes. Dysferlin and myoferlin occasionally co-localise with transferrin following retrograde antibody labelling, indicating dysferlin and myoferlin endosomes may also transit recycling pathways (indicated by **?**). Fer1L6 (red) rapidly cycles from the plasma membrane to a specific sub-compartment of the trans-Golgi network that intertwines with the recycling endosome, where it becomes intensely concentrated. Fer1L6 undergoes retrograde transit from the plasma membrane via Rab11a-positive endosomes to the trans-Golgi/recycling endosome. Only very low levels of otoferlin (orange) may be detected at the plasma membrane, though we can readily trace its endocytic passage to the trans-Golgi. Fer1L5 is an intracellular ferlin, and though shows a reticular labelling pattern, does not strongly co-label with ER markers calreticulin or calnexin.